FINITE ELEMENT SIMULATION OF THE DYNAMIC BEHAVIOR OF ADVANCED CERAMICS

G. Ruiz [(1)], C. Yu [(2)], M. Ortiz [(2)]

[(1)] **ETSI Caminos, C. y P., Universidad de Castilla-La Mancha, Pº de la Universidad 4, 13071 Ciudad Real, Spain**

[(2)] **Graduate Aeronautical Laboratories, California Institute of Technology, Pasadena, CA 91125, USA**

Abstract. This paper studies the dynamic behavior of advanced ceramics by a finite element model. It implements the direct simulation of fracture and fragmentation together with a mixed-mode cohesive law to describe the fracture process. Particularly, we simulate some dynamic Brazilian tests performed with a Hopkinson bar, at a strain rate of 75 s^{-1}, on six different materials: three kinds of alumina with different average grain sizes and degrees of purity, a blend of alumina and zirconia, silicum carbide and boron carbide. The rate dependence of the results emerges explicitly from the calculations, thanks both to the inertia attendant to the fracture process, and to the *time effect* provided by the cohesive law. Indeed, the simulations give accurate values for the dynamic strength of the six ceramics under study. The simulations also predict the main features of the crack pattern.

Resumen. Este artículo estudia el comportamiento dinámico de materiales cerámicos avanzados por medio de un modelo de elementos finitos. En particular, simulamos algunos ensayos brasileños realizados con una barra Hopkinson, a una velocidad de deformación de 75 s^{-1}, sobre seis materiales diferentes: tres tipos de alúmina con distinto tamaño de grano y grado de pureza, una mezcla de alúmina y zirconia, carburo de silicio y carburo de boro. La dependencia de los resultados a la velocidad de deformación sale explícitamente en los cálculos, gracias tanto a la inercia que acompaña al proceso de fractura como al *efecto del tiempo* dado por la ley cohesiva. De hecho, las simulaciones dan valores precisos de la resistencia a la tracción dinámica para las seis cerámicas que estudiamos. Las simulaciones también predicen los rasgos principales del patrón de fisuración.

1. INTRODUCTION

Advanced ceramics are widely used as ballistic armors due to their excellent stiffness to weight and resistance to weight ratios. Another appealing property of advanced ceramics is their capacity for dissipating energy by fracture and friction when they are comminuted by the impact of a projectile. Thus, the dynamic mechanical response of these materials is especially important to grant the required level of protection to an armor. This is why most of the scientific research in this field has focused on the determination of their dynamic properties and the development of accurate constitutive models and failure criteria at high strain rates.

In the same way as other quasi-brittle materials, advanced ceramics perform very well under compression, but their tensile strength is low, about one order of magnitude below the compressive strength. Hence most times failure takes place when the tensile strength is reached, which makes of it an essential property in the modelization of these materials. Several different tests have been proposed to measure the tensile strength of ceramics, and it has been found that it grows with the strain rate under every experimental configuration. Particularly, the diametral compression test or Brazilian test performed by means of a Hopkinson bar is seen by some experimentalists as a convenient set up giving reliable measurements.

This is the case of Rodríguez, Navarro, Sánchez-Gálvez and Gálvez, [1-3], who recently carried out a series of dynamic Brazilian tests on several advanced ceramics to show the feasibility of this experimental method to get the tensile strength at high strain rates. They studied six different materials: three aluminas (Al_2O_3) with different grain size and degree of purity, alumina blended with zirconia (Al_2O_3+ZrO_2), silicum carbide (SiC) and boron carbide (C_4B). The specimens were cylinders whose diameter and thickness were 8 and 4 mm respectively.

Here we use their results to validate a model that was originally developed for concrete undergoing the same test conditions [4]. It also gave good results studying the

propagation of dynamic cracks under mixed-mode loading [5]. It consists of a finite element model which allows fragmentation, i. e. the opening of a crack where and when tension reaches the tensile strength, and that uses a mixed-mode cohesive model to control the fracture process [6]. The simulations in this paper picture the material as linear-elastic up to fracture, while cracks respond to an irreversible cohesive law, in both cases using only the static parameters reported in the aforementioned experimental research. The rate dependence is not buried within the constitutive equations, yet it emerges explicitly from the calculations as a consequence both of the inertia of the material in the fragmentation process, and of the use of a cohesive model. Indeed, cohesive models discriminate between slow and fast rates of loading giving rise to a *time effect* [7], in a similar way as they do between small and big sizes leading to the well-known size effect [8]. The simulations not only give a good prediction of the tensile strength for each material, but also come out with crack patterns very similar to the actual ones observed in the experiments. The model predicts the formation of a principal crack that nucleates in the center of the specimen and grows towards the bearing areas, as well as some secondary cracking parallel to the main crack and near the loading areas.

The paper is organized as follows: a brief account of the main assumptions of the model and of its finite element implementation is given next. Section 3 describes the experimental set-up (3.1), the specimen geometry and material parameters (3.2), the load and boundary conditions (3.3), the mesh used in the simulations (3.4), and the simulation results (3.5). Finally, in Section 4 we draw some conclusions regarding the applicability of cohesive models to study the dynamic behavior of advanced ceramics.

2. FINITE ELEMENT MODEL

We apply the cohesive theory as in [6], during which a deformable body undergoing a motion described by a deformation mapping φ and containing a collection of cohesive cracks is contemplated. The locus of these cracks on the undeformed configuration is denoted S_o, and its unit normal **N** (Fig. 1). The jump of φ across S_o defines the opening displacement δ. We consider a simple class of mixed-mode cohesive laws accounting for tension-shear coupling obtained by an effective opening displacement:

$$\delta = \sqrt{\beta^2 \delta_s^2 + \delta_n^2} \tag{1}$$

where

$$\delta_n = \delta \cdot \mathbf{N} \tag{2}$$

is the normal opening displacement and

$$\delta_s = |\delta_s| = |\delta - \delta_n \mathbf{N}| \tag{3}$$

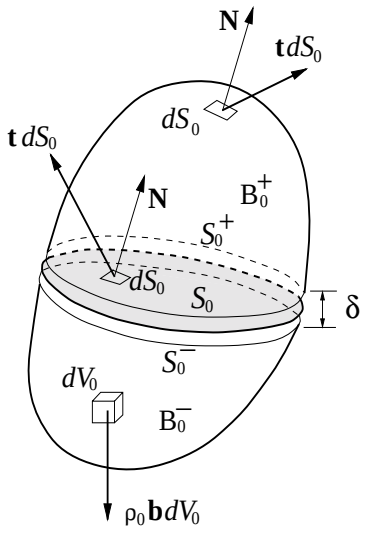

Fig. 1. Cohesive surface traversing a 3D body.

is the magnitude of the sliding displacement. The parameter β assigns different weights to the sliding and normal opening displacements. The cohesive law relates δ to a scalar effective traction:

$$t = \sqrt{\beta^{-2} |\mathbf{t}_s|^2 + t_n^2} \tag{4}$$

where $\mathbf{t}_s$ and t_n are the shear and the normal traction respectively. From (4) we also observe that β defines the ratio between the shear and the normal critical tractions.

Upon closure, the cohesive surfaces are subjected to the contact unilateral constraint, including friction. We regard contact and friction as independent phenomena to be modeled outside the cohesive law. Friction may significantly increase the sliding resistance in closed cohesive surfaces. In particular, the presence of friction may result in a steady —or even increasing— frictional resistance while the normal cohesive strength simultaneously weakens.

We assume the existence of a linearly decreasing loading envelop, as well as of a linear unloading condition to the origin (Fig. 2), giving:

$$t = \frac{t_{\max}}{\delta_{\max}} \delta \quad \text{if} \quad \delta < \delta_{\max} \quad \text{or} \quad \dot{\delta} < 0. \tag{5}$$

It is a well-known fact that cohesive theories introduce a well-defined length scale into the material description and, in consequence, are sensitive to the size of the specimen [8]. Camacho and Ortiz [7] have noted that in conjunction with inertia cohesive models introduce a *characteristic time* as well. Owing to this intrinsic time scale, the material behaves differently when subjected to fast and slow loading rates. The calculations presented subsequently demonstrate the ability of cohesive theories to account for the dynamic strength of brittle solids, i. e., the dependence of the dynamic strength on strain rate.

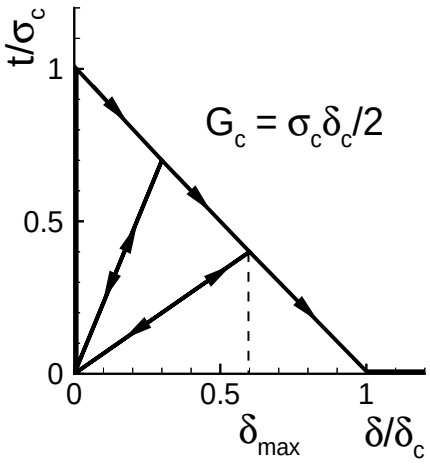

Fig. 2. Linear irreversible cohesive law.

An appealing aspect of cohesive laws as models of fracture is that they fit naturally within the conventional framework of finite element analysis. We follow Camacho and Ortiz [7] and adaptively create new surfaces as required by the cohesive model by duplicating nodes along previously coherent element boundaries. The nodes are subsequently released in accordance with the aforementioned tension-shear cohesive law. The particular class of cohesive elements used in calculations consists of two six-node triangles endowed with quadratic displacement interpolation [6].

Formulating the virtual work principle for the body and inserting the displacement interpolation into it leads to a system of semi-discrete equations of motion of the form:

$$\boldsymbol{M}\ddot{\boldsymbol{x}} + \boldsymbol{f}^{\text{int}}(\boldsymbol{x}) = \boldsymbol{f}^{ext}(t) \tag{6}$$

where $\boldsymbol{x}$ is the array of nodal coordinates, $\boldsymbol{M}$ is the mass matrix, $\boldsymbol{f}^{\text{ext}}$ is the external force array, and $\boldsymbol{f}^{\text{int}}$ is the internal force array. The second-order accurate central difference algorithm is adopted to discretize (6) in time [9].

3. SIMULATION OF THE DYNAMIC BEHAVIOR OF ADVANCED CERAMICS

3.1 Experimental set-up

The Hopkinson bar consists of an incident bar and a transmitter bar, with a short specimen placed between them, and a striker bar that impacts the incident bar to produce a longitudinal compressive pulse that propagates toward the specimen (Fig. 3a). The pulse is partially reflected in the border of the incident bar, and partially transmitted through the specimen. In this case the diametral loading generates tension perpendicular to the load plane (Fig. 3b), which eventually causes the specimen to split.

The strain records of the incident, reflected and transmitted pulses are used to calculate the corresponding stress pulses and the dynamic splitting tensile stress, f_{td}, which derives from the following equation:

$$f_{td} = \frac{2P_{\max}}{\pi WD} \tag{7}$$

where P_{max} is the maximum load transmitted through the cylinder and W and D are respectively the width and diameter of the cylinder.

3.2 Specimen geometry and material parameters

The simulations in this paper refer to experiments reported by Rodríguez, Navarro and Sánchez-Gálvez [1], Gálvez, Rodríguez and Sánchez Gálvez [2] and Gálvez [3]. The specimens are cylinders whose diameter and thickness are 8 mm and 4 mm long respectively. They tested up to six different materials: three kinds of alumina with 94, 98 and 99% degree of purity (which

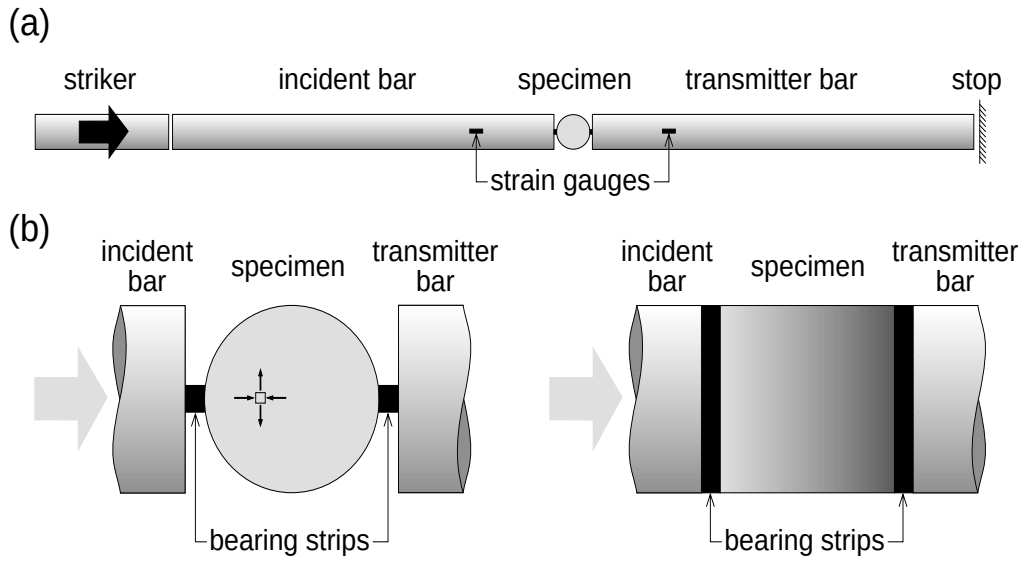

Fig. 3. Experimental set-up (a), and details of the specimen (b).

Table 1. Geometrical and static mechanical properties.

	Al_2O_3 94%	Al_2O_3 98%	Al_2O_3 99%	Al_2O_3+ZrO_2	SiC	C_4B
	A94	A98	A99	AZR		
Average grain size, (μm)	8.3	2.4	10.4	2.0	3.3	—
Density, ρ (kg/m^3)	3658	3877	3905	4027	3132	2512
Elastic modulus, E (GPa)	303	366	391	348	420	461
Tensile strength, f_{ts} (MPa)	161	179	161	155	214	211
Fracture energy, G_c (N/m)	119	98	92	162	38	88

from now on are referred to as A94, A98 and A99), a combination of alumina plus zirconia (AZR), silicum carbide (SiC) and boron carbide (B_4C). Geometrical and static mechanical properties are given in Table 1. All of them were obtained by independent tests except the fracture energy, that is estimated here from a general handbook on ceramics [10]. The coupling parameter β is taken to be 2 for all materials after some references reporting the ratio K_{IIc}/K_{Ic} for alumina and other advanced ceramics [11, 12]. The influence of the β parameter is negligible though, because the crack opens mainly in mode I [4]. The cohesive law is supposed to be linear-irreversible.

3.3 Load and boundary conditions

The tests were performed at a strain rate of 75 s^{-1}. The authors of the experimental work provided us with one full record of the stresses generated in the bars during one of the tests, which allowed calculating the rate of loading over the specimen in the simulations. In order to avoid plastic deformation in the bars, they stroke the specimens through alumina cubes whose edges were 6 mm long. There were some tests in which the cubes broke together with the specimen, but they were not considered valid.

3.4 Mesh used in the simulations

In order to make the simulations in 3D computationally efficient, we take a slice of 1/3 mm, which is 1/12 of the real thickness of the specimen, and impose plane strain boundary conditions. The mesh used in the simulation comprises 15572 nodes and 2462 10-node quadratic tetrahedra. The mesh size roughly ranges from 1/2 to 1/8 of the characteristic cohesive length of the material in the cases we are studying, and may, therefore, be expected to yield objective and mesh-size insensitive results [7]. For instance, for A99 the characteristic cohesive length is calculated to be 1.4 mm, which is about 4 times the mesh size. It is necessary to point out that the average grain size is of micrometers (see Table 1), and so capturing this length scale by choosing an element size of that order of magnitude would lead to extremely fine meshes, and subsequently to a very long computational time.

3.5 Simulation results

Selected results of the calculations and comparisons with experimental data are shown in Figs. 4, and 5. The main features of these results are discussed next.

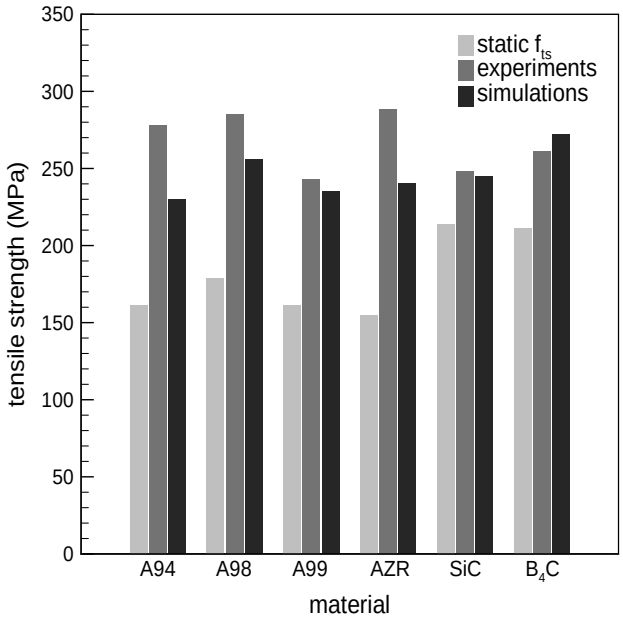

Fig. 4. Experimental and numerical dynamic tensile strength for each material, compared to their corespondent static tensile strength.

Table 2. Computed and experimental tensile strength compared to the static strength. The experimental standard deviation is shown in brackets followed by the number of tests performed for each material.

	Al_2O_3 94%	Al_2O_3 98%	Al_2O_3 99%	Al_2O_3+ZrO_2	SiC	C_4B
Tensile strength (MPa)	A94	A98	A99	AZR		
static	161 (23) 5	179 (21) 6	161 (26) 10	155 (12) 7	214 (55) 5	211 (52) 5
experiments	278 (28) 9	285 (31) 6	243 (43) 8	288 (30) 6	248 (58) 9	261 (50) 9
simulation	230	256	235	240	245	272
relative error	17%	10%	3%	17%	1%	4%

Dynamic strength and rate sensitivity

Fig. 4 compares the predicted and observed dynamic tensile strengths for all materials under consideration, and compares them with the corresponding static strengths. Table 2 provides the experimental mean value, standard deviation, and number of different tests for each material, plus the correspondent numerical value and relative error for each simulation.

The calculations capture well the overall rate-sensitivity of the materials, especially in the case of A99, SiC and B_4C, where the relative error of the computed dynamic strength is less than 5%. The accuracy of the prediction is especially noticeable having in mind that the numerical rate dependence is explicit, i. e. it emerges directly from the calculations, and all the parameters given to the model are static.

Crack pattern

The experimental crack patterns were observed by means of a high-speed camera [1-3]. A principal crack develops in the mid-plane of the cylinder at a very fast speed and approximately at the peak load, as Fig. 5a shows for a B_4C specimen. Secondary cracks, parallel to the main diametral crack, also appear as the load decreases, leading to the typical columnar failure of Brazilian tests. Some cracking near the supports is also observed in the shots taken after the load peak.

The predicted sequence of crack patterns follows closely the experimental patterns described above. Fig. 5b shows the deformed mesh at the load peak —the displacements are magnified by a factor of 100 in order to aid visualization—. The main diametral crack is fully developed in the figure, whereas the secondary cracks are just initiating. The simulations also report some additional damage near the supports, although the cracks cannot be distinguished in Fig. 5b yet.

4. SUMMARY AND CONCLUSIONS

We used cohesive theories of fracture, in conjunction with the direct simulation of fracture and fragmentation, to describe processes of tensile damage and compressive crushing in advanced ceramics subjected to dynamic loading. The configuration contemplated in this study is the Brazilian cylinder test performed in a Hopkinson bar, which has been proposed as a convenient and reliable experimental method to obtain the dynamic tensile strength of these materials. Our approach accounts explicitly for the development of macroscopic cracks, and uses a mixed-mode cohesive law to control the fragmentation process. The effective dynamic behavior of six different types of advanced ceramics is *predicted* as an outcome of the calculations. In particular, our simulations capture closely the experimentally observed rate-sensitivity of the dynamic strength of advanced ceramics, i. e., the increase in dynamic strength with strain-rate. The model also predicts key features of the fracture pattern such as the primary cracks parallel to the load plane, as well as the secondary profuse cracking near the supports.

We have assumed that the cohesive properties of the material are rate-independent and therefore determined by static properties such as the static tensile strength. However, we have noted that cohesive theories, in addition to building a characteristic length into the material description, endow the material with an intrinsic *time scale* as well. This intrinsic time scale accounts for the ability of the model to predict key aspects of the dynamic behavior of advanced ceramics, such as the strain-rate sensitivity of the tensile strength.

5. ACKNOWLEDGEMENTS

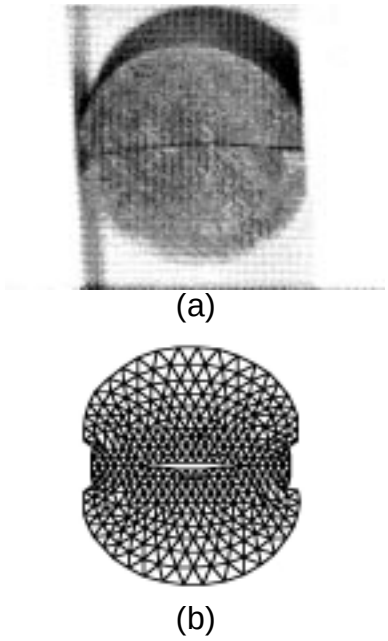

Fig. 5. (a) Snapshot of the main crack appearing at the peak load in a B_4C specimen (b) compared to its numeric counterpart.

Gonzalo Ruiz gratefully acknowledges partial financial support for a short stay at the *California Institute of Technology* provided by the *Vicerrectorado de Investigación* of the *Universidad de Castilla-La Mancha*. We are thankful to Dr. Gálvez and Prof. Rodríguez for providing us with some records of their tests and some insights into their excellent experimental work.

6. REFERENCES

[1] Rodríguez J, Navarro C and Sánchez-Gálvez V, "Splitting tests: an alternative to determine the dynamic tensile strength of ceramic materials", Journal de Physique IV **4** (C8), 101-106 (1994).

[2] Gálvez F, Rodríguez J and Sánchez-Gálvez V, "Tensile strength measurements of ceramic materials at high rates of strain", Journal de Physique IV C3, 151-156 (1997).

[3] Gálvez F, "Caracterización mecánica de materiales cerámicos avanzados a altas velocidades de deformación", Ph. D. Thesis, Departamento de Motopropulsión y Fluidodinámica, E.T.S. de Ingenieros Aeronáuticos, Universidad Politécnica de Madrid (1999).

[4] Ruiz G, Ortiz M and Pandolfi A, "Three-dimensional finite-element simulation of the dynamic Brazilian tests on concrete cylinders", International Journal for Numerical Methods in Engineering **48**, 963-994 (2000).

[5] Ruiz G, Pandolfi A and Ortiz M, "Three-dimensional cohesive modeling of dynamic mixed-mode fracture", International Journal for Numerical Methods in Engineering, special USACM Congress Issue, in press.

[6] Ortiz M and Pandolfi A, "Finite-deformation irreversible cohesive elements for three-dimensional crack-propagation analysis", International Journal for Numerical Methods in Engineering **44**, 1267-1282 (1999).

[7] Camacho GT and Ortiz M, "Computational modeling of impact damage in brittle materials", International Journal of Solids and Structures **33** (20-22), 2899-2938 (1996).

[8] Bazant ZP and Planas J, "Fracture and size effect in concrete and other quasi-brittle materials", CRC Press, Boca Raton FL (1998).

[9] Hughes TJR, "The finite element method: linear static and dynamic finite element analysis", Prentice Hall, Englewood Cliffs NJ (1987).

[10] Schneider SJ (Technical Chairman) "Engineered materials handbook. Volume 4: Ceramics and glasses". ASM International, (1991).

[11] Shetty DK, Rosenfield AR,and Duchworth WH, "Mixed-mode fracture of ceramics in diametral compression", Journal of the American Ceramic Society 69 (6), 437-443 (1986).

[12] Tikare V and Choi SR, "Combined mode I and mode II fracture of monolithic ceramics", Journal of the American Ceramic Society **76** (9), 2265-2272 (1993).